Chirality-selective proximity effect between chiral *p*-wave superconductors and quantum Hall insulators

Ryota Nakai,[1] Koji Kudo,[2] Hiroki Isobe,[2] and Kentaro Nomura[2]
[1]*RIKEN Center for Quantum Computing (RQC), Wako, Saitama 351-0198, Japan*
[2]*Department of Physics, Kyushu University, Fukuoka 819-0395, Japan*

(Received 14 May 2025; accepted 5 September 2025; published 25 September 2025)

Heterostructures of superconductors and quantum-Hall insulators are promising platforms for topological quantum computation. However, these two systems are incompatible in some aspects, such as a strong magnetic field, the Meissner effect, and chirality. In this work, we address the condition that the superconducting proximity effect works in the bulk of quantum Hall states, and identify an essential role played by the vortex lattice regardless of pairing symmetry. We extend this finding to a heterostructure between a chiral *p*-wave superconductor in the mixed state and an integer quantum Hall insulator. The proximity effect works selectively in the lowest Landau level, depending on relative chiralities. If the chiralities align, a topological phase transition to a topological superconductor occurs.

DOI: 10.1103/qxt1-ncfn

I. INTRODUCTION

Topology and pairing are the key to the creation of non-Abelian anyons. Specifically, Majorana zero modes [1–3], an example of these non-Abelian anyons, appear in, e.g., superfluid ^{3}He [4], the Moore-Read fractional quantum Hall (QH) state [5,6], unconventional superconductors (SCs) [7,8], and quantum spin liquids [9]. All these systems have a nontrivial topology and intrinsic pairing of atoms, composite fermions [10], electrons, and emergent fermions, respectively. On the other hand, it is also possible to induce pairing extrinsically via the superconducting proximity effect by making a heterostructure with SCs. There are a variety of proposals for creating Majorana zero modes in heterostructures of *s*-wave SCs with, e.g., topological insulators [11–13], quantum anomalous Hall insulators [14], Rashba nanowires [8,15–18], and magnetic atomic chains [19–26].

The proximity effect creates a correlation between electrons and holes through penetrating Cooper pairs from SCs. However, a proximitized SC does not necessarily induce the proximity effect. This is because, in addition to microscopic details of the interface, the proximity effect is subject to the limitation as to whether electronic states in the non-SC side can accommodate Cooper pairs. Specifically, singlet Cooper pairs cannot penetrate spin-polarized materials such as half metals because of the spin configuration [27–29], nor can they penetrate magnetic Weyl semimetals because of the opposite chirality of the nodes, known as the chirality blockade [30]. Bulk QH states are another example, as we will explain in the following.

SC/QH heterostructures have been proposed as a platform for more exotic non-Abelian anyons such as parafermions and Fibonacci anyons [31–34]. There are roughly two configurations of the heterostructure depending on whether an SC is attached to the QH edge, or it covers the entire bulk. Theoretical and experimental studies so far have paid particular attention to the former configuration with integer [35–62] and fractional [31–34,63–65] QH edges, since the edge is the only conduction channel. In contrast, for the latter configuration, there are possibly three factors that spoil the functionality of SC/QH heterostructures. (i) QH states require a strong magnetic field, which is likely to break superconductivity [66,67]. (ii) Even if superconductivity is retained, the Meissner effect repels the magnetic field, making QH states difficult to realize. (iii) If pairing is *s*-wave, Cooper pairs are formed between time-reversal pairs of electrons, while QH states break time-reversal symmetry. Nonetheless, it has been shown that a bulk QH state coupled with a mixed-state *s*-wave pair potential shows a topological phase transition to topological SCs [68–71].

The purpose of this study is twofold: to elucidate the condition that the *s*-wave and *p*-wave proximity effect works in the bulk QH states, and to study the topological properties of a heterostructure of a mixed-state chiral *p*-wave SC and a QH insulator. As for the former purpose, we will show that the angular momentum of the Cooper pairs generated by the vortex lattice is necessary to pair the bulk QH states. This consequence is true regardless of whether pairing symmetry is *s*-wave or *p*-wave. Though the *s*-wave case has been studied in Refs. [69,70], we will recast their study in the disk geometry to make the chiral nature of the heterostructure explicit and then extend the argument to the *p*-wave case. Based on this finding, we consider a heterostructure of a mixed-state chiral *p*-wave SC and a QH insulator. The two systems in this heterostructure have different kinds of chirality, that is, the sign of the Cooper pairs' angular momentum, which is $\pm\hbar$ for $p_x \pm ip_y$ wave and the chirality of the Landau levels. The proximity effect works selectively depending on the relative alignment of the chiralities, particularly in the lowest Landau level (LLL). With an effective chiral *p*-wave pair potential, the LLL shows a topological phase transition to a topological SC.

Notice that a chiral *p*-wave SC is itself a topological SC. However, we can distinguish between the topological superconductivity of a chiral *p*-wave SC and that induced in a QH

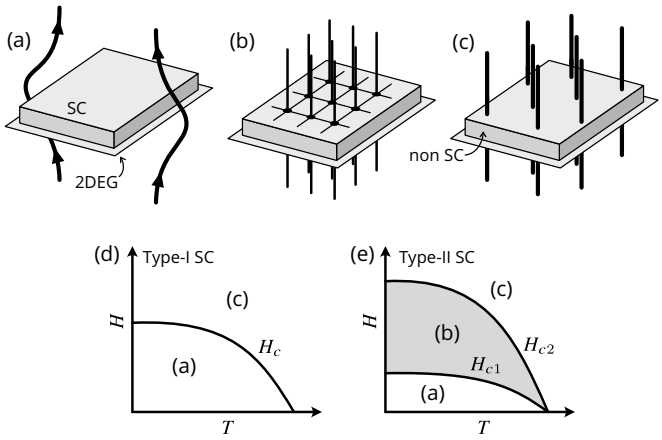

FIG. 1. A heterostructure of a type-I or type-II superconductor and a quantum Hall insulator (a) below H_c or H_{c1} where the magnetic field is completely screened by the Meissner effect, (b) in the mixed state between H_{c1} and H_{c2} where the vortex lattice is formed, and (c) above H_c or H_{c2} where superconductivity is broken. (d), (e) The corresponding phases in the phase diagrams of type-I and type-II superconductors, respectively.

insulator (we will show this in Sec. III D). For the purpose of creating more exotic anyons, the latter topological superconductivity is preferred, since some proposals require the combination of fractional charges and pairing [31–34]. The emergence of proximity-induced topological superconductivity in an integer QH insulator is the first step toward this direction.

The rest of this paper is organized as follows. In Sec. II, we first give a phenomenological argument on an SC/QH heterostructure in a magnetic field, and show that, by using a continuum model on a disk, an impractical setup with s-wave SCs does not result in the bulk proximity effect. Then, we recast the works in Refs. [69,70] in a disk geometry and show the necessity of the vortex lattice for the s-wave case. In Sec. III, we show that the same problem arises with chiral p-wave SCs, but is resolved by mixed-state SCs. In Sec. IV, we confirm these results using a tight-binding model. Finally, we conclude in Sec. V.

II. PRELIMINARIES

A. SC/QH insulator heterostructure

Throughout this paper, we consider heterostructures where the bulk of a two-dimensional electron gas is covered by an SC and a strong perpendicular magnetic field is applied.

First, we focus on the SC side [72]. An SC subject to a strong magnetic field is in one of the following three cases: (a) below H_c in type-I SCs or below H_{c1} in type-II SCs, the magnetic field is screened by the Meissner effect, (b) between H_{c1} and H_{c2} in type-II SCs, the magnetic field penetrates the SC as a vortex lattice, or (c) above H_c in type-I SCs or above H_{c2} in type-II SCs, the superconductivity is lost (Fig. 1). In each phase, the pair potential $\Delta(\boldsymbol{r})$ and the magnetic field $B(\boldsymbol{r})$ are (a) $|\Delta(\boldsymbol{r})| = \Delta_0$ and $B(\boldsymbol{r}) = 0$, (b) $|\Delta(\boldsymbol{r})| < \Delta_0$ but nonzero and $B(\boldsymbol{r}) \neq 0$, (c) $|\Delta(\boldsymbol{r})| = 0$ and $B(\boldsymbol{r}) = H$, where Δ_0 is the pair potential of an SC below H_c or H_{c1}. We here set the permeability $\mu_0 = 1$.

As for the two-dimensional electron gas side, we need both the strong magnetic field and the proximity effect to construct an SC/QH insulator heterostructure. Either one of them is lost in the cases (a) and (c). The remaining possibility is the case (b). However, even in the presence of both the magnetic field and the superconductivity, it is nontrivial whether the proximity effect works in QH insulators. One of the main claims of this work is that the case (b) is essential, regarding not just the presence of both superconductivity and a magnetic field but also for the proximity effect. In Secs. II C and III, we will discuss the condition of the presence of the proximity effect in QH states from the viewpoint of the angular momentum. Before that, we will review in the next subsection that a uniform pair potential in a QH insulator, which would be the simplest theoretical assumption but is not listed in Fig. 1, fails to induce the bulk proximity effect.

B. Uniform s-wave pair potential

The Hamiltonian of a continuum model of a spinful but spin-unpolarized QH insulator on a disk that couples with an s-wave pair potential $\Delta(\boldsymbol{r})$ is given by $H^s = H_0^{\text{spinful}} + H_\Delta^s$, where

$$H_0^{\text{spinful}} = \sum_{\sigma=\uparrow,\downarrow} \int d\boldsymbol{r} \psi_\sigma^\dagger(\boldsymbol{r}) h_0(\boldsymbol{r}) \psi_\sigma(\boldsymbol{r}), \tag{1}$$

$$H_\Delta^s = \int d\boldsymbol{r} \psi_\uparrow^\dagger(\boldsymbol{r}) \Delta(\boldsymbol{r}) \psi_\downarrow^\dagger(\boldsymbol{r}) + \text{H.c.} \tag{2}$$

and

$$h_0(\boldsymbol{r}) = \frac{(-i\hbar\boldsymbol{\partial} + e\boldsymbol{A})^2}{2m_e} - \mu, \tag{3}$$

where m_e is the electron mass, $-e < 0$ is the electron charge, μ is the chemical potential, and we employ the symmetric gauge $\boldsymbol{A} = (-By/2, Bx/2)$. $\psi_\sigma(\boldsymbol{r})$ is the electron annihilation operator of spin σ. We assume that the Zeeman term is negligible because of a small g-factor. The simultaneous eigenstate of the normal-state Hamiltonian $h_0(\boldsymbol{r})$ with eigenvalue $\hbar\omega_c(n+1/2)$ ($n \in \mathbb{Z}, n \geqslant 0, \omega_c = eB/m_e$) and the angular momentum operator with eigenvalue $-\hbar m$ ($m \in \mathbb{Z}, m \geqslant -n$) is given by the Landau level wavefunction [73]

$$\begin{aligned}\phi_{nm}(\boldsymbol{r}) &= \frac{a^{\dagger n} b^{\dagger n+m}}{\sqrt{n!(n+m)!}} \phi_{00}(\boldsymbol{r}) \\ &= \frac{(-1)^n}{\sqrt{2\pi}\ell_B} \sqrt{\frac{n!}{2^m(n+m)!}} \left(\frac{z}{\ell_B}\right)^m e^{-z\bar{z}/4\ell_B^2} L_n^m\left(\frac{z\bar{z}}{2\ell_B^2}\right),\end{aligned} \tag{4}$$

where $\ell_B = \sqrt{\hbar/eB}$, $\phi_{00} = e^{-z\bar{z}/4\ell_B^2}/\sqrt{2\pi}\ell_B$, $z = x - iy$, L_n^m is the associated Laguerre polynomial, and

$$a = \frac{1}{\sqrt{2}}\left(2\ell_B\partial_{\bar{z}} + \frac{z}{2\ell_B}\right), \quad b = \frac{1}{\sqrt{2}}\left(2\ell_B\partial_z + \frac{\bar{z}}{2\ell_B}\right). \tag{5}$$

On the Landau level basis $\phi_{nm}(\boldsymbol{r})$ with $\psi_\sigma(\boldsymbol{r}) = \sum_{nm}\phi_{nm}(\boldsymbol{r})c_{nm\sigma}$, the pairing Hamiltonian is written as

$$H^s_\Delta = \sum_{nmn'm'} \Delta^s_{nmn'm'} c^\dagger_{nm\uparrow} c^\dagger_{n'm'\downarrow} + \text{H.c.}, \tag{6}$$

where the matrix element is

$$\Delta^s_{nmn'm'} = \int d\boldsymbol{r}\phi^*_{nm}(\boldsymbol{r})\Delta(\boldsymbol{r})\phi^*_{n'm'}(\boldsymbol{r}). \tag{7}$$

Since $a^* = b$, the complex conjugation of ϕ_{nm} can be obtained by interchanging $a^\dagger$ and $b^\dagger$ in (4), which gives $\phi^*_{nm} = \phi_{n+m,-m}$. With this identity, the matrix element for a uniform pair amplitude $\Delta(\boldsymbol{r}) = \Delta_0$ gives

$$\Delta^s_{nmn'm'} = \Delta_0\delta_{n,n'+m'}\delta_{n+m,n'}. \tag{8}$$

Projecting onto the LLL by $n = n' = 0$, the pairing Hamiltonian reduces to

$$H^s_\Delta \to \Delta_0 c^\dagger_{00\uparrow} c^\dagger_{00\downarrow} + \text{H.c.} \tag{9}$$

This implies that only spin-up and spin-down electrons with angular momentum 0 can make a Cooper pair by the proximity effect from a uniform s-wave SC. The same conclusion holds for higher Landau levels if pairing is restricted within a single Landau level.

This result can be understood from the perspective of the angular momentum. The angular momentum of an s-wave Cooper pair is 0 and that of the LLL state electrons is 0 or negative. As a result, possible pairing is between electrons with angular momentum 0. Indeed, since $\phi^*_{0m}\phi^*_{0m'}$ contains $\bar{z}^{m+m'}$, the angular integral in (7) gives 0 unless $m = m' = 0$. Macroscopically, the amount of induced Cooper pairs in the LLL is negligible in the thermodynamic limit, and hence we cannot anticipate topological phase transitions.

In addition, the above proximity effect breaks spatial translation symmetry. Specifically, the LLL state with m is distributed around a circle of radius $\sqrt{2m}\ell_B$. This indicates that the uniform s-wave pair potential works only at the center ($m = 0$) of the disk, which is compatible with the vanishing proximity effect in the thermodynamic limit. Similar things happen in different gauges and geometries. With the Landau gauge and the cylinder geometry, the uniform pair potential works dominantly for $k = 0$ states (Appendix B), and with the Dirac monopole's gauge and the spherical geometry, it works at the north and south poles. In our setup, this problem is considered to be a result of an impractical setup, that is, a uniform s-wave pair potential is applied in a QH insulator, which is not listed in Fig. 1.

C. Mixed-state s-wave pair potentials

In a mixed-state SC, quantized magnetic fluxes $h/2e$ form the Abrikosov lattice. Each flux is screened by supercurrent flowing around a vortex, which results in a center-of-mass angular momentum of the Cooper pairs. The Cooper pairs can have a variety of total angular momentum, which is the sum of the relative and center-of-mass ones. This removes the constraint by the angular momentum in QH insulators. The s-wave case corresponds to Refs. [68–71]. We review their system from the viewpoint of the angular momentum. Notice that, in the following, we assume that the magnetic field is spatially uniform because of a long penetration depth compared with the distance between neighboring vortices slightly below H_{c2}.

The pair potential $\Psi(\boldsymbol{r})$ of SCs close to H_{c2} obeys the linearized Ginzburg-Landau equation [72]

$$\left[\frac{(-i\hbar\boldsymbol{\partial} + e^*\boldsymbol{A})}{2m^*_e} + \alpha\right]\Psi(\boldsymbol{r}) = 0, \tag{10}$$

where $e^* = 2e$, $m^*_e = 2m_e$, and $\alpha < 0$. This equation is the same as that of electrons except that the mass and charges are those of Cooper pairs. The pair potential is written in terms of the LLL wavefunctions of Cooper pairs. Assuming that the pair potential $\Delta(\boldsymbol{r})$ induced in a QH insulator is proportional to $\Psi(\boldsymbol{r})$, we have

$$\Delta(\boldsymbol{r}) = \sum_{m\geqslant 0}\frac{C_m}{\sqrt{\pi m!}\ell_B}\left(\frac{z}{\ell_B}\right)^m e^{-z\bar{z}/2\ell^2_B}. \tag{11}$$

Each wavefunction is characterized by the angular momentum $-m\hbar$, which is distributed around a circle of radius $\sqrt{m}\ell_B$. The magnitude of C_m is approximately $|C_m| \simeq \ell_B\sqrt{\pi\langle|\Delta(\boldsymbol{r})|^2\rangle}$ irrespective of m, where $\langle\cdots\rangle$ denotes the spatial average (Appendix A). We note that $\Delta(\boldsymbol{r})$ is slowly varying on the vortex lattice scale slightly below H_{c2}. The pair potential (11) contains m_0 vortices when the summation of the right-hand side is truncated to m_0. However, the position of the vortices depends on C_m, which is determined to minimize the Ginzburg-Landau free energy [72].

QH states can form an extensive number of Cooper pairs by (11). Specifically, the matrix element between the LLL states is given by (Appendix A)

$$\Delta^s_{0m0m'} = \frac{C_{m+m'}}{2\sqrt{\pi}\ell_B}\sqrt{\frac{(m+m')!}{2^{m+m'}m!m'!}}. \tag{12}$$

The matrix element (12) with a fixed $m + m'$ is maximized when $|m - m'|$ is minimized. This is because there is a substantial overlap between the Cooper pair wavefunction with angular momentum $-2m\hbar$ and the electronic LLL wavefunction with angular momentum $-m\hbar$, since they are distributed along the same circle of radius $\sqrt{2m}\ell_B$. In addition, the angular dependence of $\bar{z}^{2m}$ in $\phi^*_{0m}\phi^*_{0m}$ is canceled by that of z^{2m} in $\Delta(\boldsymbol{r})$, which makes the integral (7) nonvanishing. The mixed-state pair potential works as a glue to the Landau level states. A similar discussion at a QH edge coupled with a Rashba SC has been given in Ref. [53].

III. CONTINUUM MODEL

In this section, we identify the necessity of the vortex lattice by considering the proximity effect from a uniform and mixed-state chiral p-wave pair potentials, where time-reversal symmetry is broken as in QH insulators.

A. A relation between s-wave and chiral p-wave pair potentials

First, we derive a general relation between the matrix elements of the s-wave and chiral p-wave pair potentials. The Hamiltonian of a spinless QH insulator coupled with a

spinless chiral p-wave pair potential is given by $H^{p_x\pm ip_y} = H_0^{\text{spinless}} + H_\Delta^{p_x\pm ip_y}$, where

$$H_0^{\text{spinless}} = \int d\boldsymbol{r}\psi^\dagger(\boldsymbol{r})h_0(\boldsymbol{r})\psi(\boldsymbol{r}), \tag{13}$$

$$H_\Delta^{p_x\pm ip_y} = \frac{1}{2}\int d\boldsymbol{r}\psi^\dagger(\boldsymbol{r})\frac{\{-i\hbar\partial_\pm, \Delta(\boldsymbol{r})\}}{2}\psi^\dagger(\boldsymbol{r}) + \text{H.c.}, \tag{14}$$

and $\partial_\pm \equiv \partial_x \pm i\partial_y$. $\psi(\boldsymbol{r})$ is the electron annihilation operator. On the Landau level basis, the pairing Hamiltonian is rewritten as

$$H_\Delta^{p_x\pm ip_y} = \sum_{nmn'm'} \Delta_{nmn'm'}^{p_x\pm ip_y} c_{nm}^\dagger c_{n'm'}^\dagger + \text{H.c.} \tag{15}$$

We can replace derivatives in (14) by the covariant derivatives as

$$\Delta_{nmn'm'}^{p_x\pm ip_y} = \frac{1}{2}\int d\boldsymbol{r}\phi_{nm}^* \frac{-i\hbar D_\pm^h\Delta + \Delta(-i\hbar D_\pm^e)}{2}\phi_{n'm'}^*, \tag{16}$$

where $-i\hbar D_\alpha^{e/h} = -i\hbar\partial_\alpha \pm eA_\alpha$ ($\alpha = \pm$, $A_\pm \equiv A_x \pm iA_y$) is the covariant derivative for electrons and holes, respectively. Different types of the covariant derivatives appear in (16) owing to the gauge invariance. Each term of (16) is invariant under a gauge transformation

$$\begin{aligned}\phi_{nm}(\boldsymbol{r}) &\to e^{ie\chi(\boldsymbol{r})/\hbar}\phi_{nm}(\boldsymbol{r}),\\ \Delta(\boldsymbol{r}) &\to e^{2ie\chi(\boldsymbol{r})/\hbar}\Delta(\boldsymbol{r}),\\ \boldsymbol{A}(\boldsymbol{r}) &\to \boldsymbol{A}(\boldsymbol{r}) - \boldsymbol{\partial}\chi(\boldsymbol{r}).\end{aligned}$$

Since ϕ_{nm}^* and $\phi_{n'm'}^*$ transform like holes, while $\phi_{nm}^*\Delta$ and $\Delta\phi_{n'm'}^*$ transform like electrons, the derivative of the first (second) term should transform like that for holes (electrons). The electron covariant derivative acts like raising or lowering operator as

$$-i\hbar D_\pm^e\phi_{nm} = \frac{\sqrt{2}i\hbar}{\ell_B}\begin{cases}\sqrt{n+1}\phi_{n+1m-1} & (+)\\ -\sqrt{n}\phi_{n-1m+1} & (-)\end{cases}, \tag{17}$$

where we define $\phi_{nm} = 0$ with $n < 0$. With this result, the matrix elements of the s-wave and chiral p-wave pair potentials with a common $\Delta(\boldsymbol{r})$ are related by

$$\Delta_{nmn'm'}^{p_x\pm ip_y} = -\frac{i\hbar}{2\sqrt{2}\ell_B}\begin{cases}-\sqrt{n}\Delta_{n-1m+1n'm'}^s + \sqrt{n'}\Delta_{nmn'-1m'+1}^s & (p_x+ip_y)\\ \sqrt{n+1}\Delta_{n+1m-1n'm'}^s - \sqrt{n'+1}\Delta_{nmn'+1m'-1}^s & (p_x-ip_y)\end{cases}. \tag{18}$$

Here, $\Delta_{nmn'm'}^s$ is given in (7).

B. Uniform chiral p-wave pair potential

The absence of the bulk proximity effect from uniform SCs is true even if we consider a chiral p-wave pair potential. For a uniform chiral p-wave pair potential $\Delta(\boldsymbol{r}) = \Delta_0$, one can evaluate the matrix element by (8) and (18). Projecting onto the LLL, we have

$$H_\Delta^{p_x\pm ip_y} \to \begin{cases}0 & (p_x+ip_y)\\ \frac{i\hbar\Delta_0}{\sqrt{2}\ell_B}c_{01}^\dagger c_{00}^\dagger + \text{H.c.} & (p_x-ip_y)\end{cases}. \tag{19}$$

This implies that the proximity effect does not work in the LLL from $p_x + ip_y$-wave SCs, while that from $p_x - ip_y$ SCs couples electrons with angular momentum $m = 0$ and 1. Since the relative angular momentum of the Cooper pairs is $\pm\hbar$ in $p_x \pm ip_y$-wave SCs, the pairing between $m = 0$ and 1 is possible by the $p_x - ip_y$-wave pair potential. Importantly, the proximity effect from uniform SCs, regardless of whether pairing symmetry is s-wave or p-wave does not induce a bulk proximity effect in QH insulators, and is negligible in the thermodynamic limit.

C. Mixed-state chiral p-wave pair potentials

What is new about considering a mixed-state chiral p-wave pair potential is that the pair potential on the LLL depends on the relative chirality. The matrix element of a mixed-state chiral p-wave pair potential in the LLL is readily obtained by (18) given the function $\Delta(\boldsymbol{r})$ is the same as the s-wave case [Eq. (11)]. As in the uniform case, the $p_x + ip_y$-wave pair potential does not work in the LLL ($\Delta_{0m0m'}^{p_x+ip_y} = 0$), while the $p_x - ip_y$-wave pair potential is given by (see Appendix A for derivation)

$$\Delta_{0m0m'}^{p_x-ip_y} = C_{m+m'-1}\frac{i\hbar(m-m')}{4\sqrt{\pi}\ell_B^2}\sqrt{\frac{(m+m'-1)!}{2^{m+m'}m!m'!}}. \tag{20}$$

This is one of the main results of this work. While LLL states with the same m cannot make pairs because of the Pauli's exclusion principle (we assumed spinless chiral p-wave pairing), those with smaller $|m-m'|$ but $m \neq m'$ are likely to form Cooper pairs.

From the perspective of the angular momentum, the chirality dependence is not obvious. As the center-of-mass angular momentum is the same for all pairing symmetries, the presence and absence of the proximity effect on the LLL is not restricted by the angular momentum but the chirality of the p-wave pair potential. Indeed, the proximity effect from both chiralities do work in higher Landau levels. We will examine the above result in a lattice model in Sec. IV. Notice that it is one of the advantages of considering the disk geometry that the chirality of the pairing and that of the center-of-mass motion can be discussed on the same footing.

In our heterostructure, distinct chiralities are attributed to three types of motions, that is, the center-of-mass motion of Cooper pairs determined by the Ginzburg-Landau equation, the relative motion of Cooper pairs that is $\pm\hbar$ for $p_x \pm ip_y$ wave, and that of QH states. Suppose we flip the direction of the applied magnetic field, the chirality of the center-of-mass motion and the QH states are flipped by definition. On the other hand, the chirality of pairing symmetry is not strictly tied to the applied magnetic field, but it depends energetically on the direction of the field [74]. As a result, the same phenomenon with the opposite chirality would occur upon flipping the direction of the magnetic field.

D. Chern number

Before we proceed to the lattice model, we review our heterostructures from the perspective of the Chern number. The purpose of this subsection is to show that the emergence of topological superconductivity in a chiral p-wave SC/QH insulator heterostructure is a consequence of a topological phase transition in the QH insulator. We can distinguish between the topological superconductivity intrinsic to a chiral p-wave SC and that induced in a QH insulator. Throughout this paper, we use the Bogoliubov-de Gennes (BdG) Chern number $\mathcal{N}$ of the quasi-hole bands. Here, we assume a periodic boundary condition in both the x and y directions. Let the eigenspinor $\eta_{j\boldsymbol{k}}$ of the momentum-space BdG Hamiltonian $h(\boldsymbol{k})$ be specified by the band number j and the momentum $\boldsymbol{k}$. The BdG Chern number of a band j is the integral of the Berry curvature over the Brillouin zone

$$\mathcal{N}_j = \frac{1}{2\pi}\int_{\mathrm{BZ}} d\boldsymbol{k}[\nabla_{\boldsymbol{k}} \times \boldsymbol{A}_j(\boldsymbol{k})]_z, \tag{21}$$

where $\boldsymbol{A}_j(\boldsymbol{k}) = -i\eta^\dagger_{j\boldsymbol{k}}\nabla_{\boldsymbol{k}}\eta_{j\boldsymbol{k}}$. The BdG Chern number $\mathcal{N}$ of the quasi-hole bands is defined by the summation of $\mathcal{N}_j$ over the negative-energy bands. In nonsuperconducting systems, the BdG Chern number is twice the usual Chern number, e.g., $\mathcal{N} = 2$ when the spin-polarized LLL is filled.

First, we review the BdG Chern number of the mixed-state s-wave SC/QH insulator heterostructure [69–71]. A mixed-state s-wave superconductor has $\mathcal{N} = 0$ while a QH insulator has $\mathcal{N} = 2$, and hence the total BdG Chern number without the proximity effect is $\mathcal{N} = 2$. With the proximity effect, the QH state can become a topological superconductor with odd $\mathcal{N}$. The total BdG Chern number after the topological phase transition is, of course, odd. This indicates that the appearance of topological superconductivity (odd total $\mathcal{N}$) can be attributed to the proximity-induced topological phase transition in a QH insulator.

A similar story holds in a mixed-state chiral p-wave SC/QH insulator heterostructure. The caveat here is that mixed-state chiral p-wave SCs have even $\mathcal{N}$ [74,75]. Each isolated vortex in chiral p-wave SCs binds topologically a Majorana zero mode [7]. When two or more vortices are getting closer, the bound Majorana fermions start tunneling between them. When vortices form a uniform lattice, the Majorana fermions form energy bands inside the superconducting energy gap. What Refs. [74,75] have shown was that the tight-binding model of tunneling Majorana fermions is written as a π-flux model, and thus the gapped subband have odd $\mathcal{N}$. Together with the chiral p-wave condensate's odd BdG Chern number, the mixed-state chiral p-wave SCs have even $\mathcal{N}$. Therefore, the Chern-number argument for the mixed-state s-wave case also applies to the mixed-state chiral p-wave case, that is, an odd total $\mathcal{N}$ is attributed to the proximity-induced topological phase transition in a QH insulator. In other words, the topological SC phase in the chiral p-wave SC cannot be continuously connected to the induced one in a QH insulator.

Notice, however, that the Chern number of the mixed-state chiral p-wave SCs in Refs. [74,75] has been evaluated away from H_{c2}. Specifically, they used a pair potential $\Delta_0 e^{i\theta(\boldsymbol{r})}$ that has spatially uniform absolute value and the phase $\theta(\boldsymbol{r})$ determined by the London equations

$$\boldsymbol{\partial} \times \boldsymbol{\partial}\theta(\boldsymbol{r}) = 2\pi\hat{z}\sum_j \delta(\boldsymbol{r} - \boldsymbol{r}_j), \quad \boldsymbol{\partial}^2\theta(\boldsymbol{r}) = 0, \tag{22}$$

where $\boldsymbol{r}_j$ is the center of a vortex. This form of the pair potential is valid when $H \ll H_{c2}$ where the distance between neighboring vortices is much longer than the coherence length. Since our focus is a region close to H_{c2}, we examine whether the conclusion in Refs. [74,75] is true even near H_{c2} in the next section.

IV. LATTICE MODEL

In this section, we examine the following three points using tight-binding models of two systems, a chiral p-wave SC and a chiral p-wave SC/QH insulator heterostructure: (i) the BdG Chern number of a mixed-state chiral p-wave SC is even, (ii) the proximity effect in the LLL depends on the chirality of the p-wave pair potential, and (iii) a topological superconductivity appears in the heterostructure. Notice that the following calculations are done under the periodic boundary condition in both x and y directions. We confirmed the same conclusions for the continuum model on a cylinder as that on a disk (see Appendix B).

A. Tight-binding model

We consider a common square-lattice tight-binding Hamiltonian for the chiral p-wave SC and the QH insulator, which is given by

$$H = -\sum_{\boldsymbol{r}\boldsymbol{\delta}} t_{\boldsymbol{r}\boldsymbol{r}+\boldsymbol{\delta}} c^\dagger_{\boldsymbol{r}} c_{\boldsymbol{r}+\boldsymbol{\delta}} - \mu\sum_{\boldsymbol{r}} c^\dagger_{\boldsymbol{r}} c_{\boldsymbol{r}} + \frac{1}{2}\sum_{\boldsymbol{r}\boldsymbol{\delta}} (\Delta_{\boldsymbol{r}\boldsymbol{r}+\boldsymbol{\delta}} c^\dagger_{\boldsymbol{r}} c^\dagger_{\boldsymbol{r}+\boldsymbol{\delta}} + \mathrm{H.c.}), \tag{23}$$

where $\boldsymbol{r} \in \mathbb{Z}^2$, $\boldsymbol{\delta} = \pm\hat{x}$ or $\pm\hat{y}$ and the lattice constant is set to 1. The chiral p-wave pair potential is $\Delta_{\boldsymbol{r}\boldsymbol{r}+\boldsymbol{\delta}} = \Delta(\boldsymbol{r} + \boldsymbol{\delta}/2)s_{\boldsymbol{\delta}}$, where $s_{\pm\hat{x}} = \mp i$, $s_{\pm\hat{y}} = \pm C$, and the chirality $C = \pm 1$ corresponds to the $p_x \pm ip_y$ pairing. The magnetic unit cell size is $N_x \times N_y$. The nearest-neighbor hopping amplitude is subject to a magnetic flux ϕ_0/N_xN_y per plaquette, where $\phi_0 = h/e$, and hence $t_{\boldsymbol{r}\boldsymbol{r}\pm\hat{x}} = t$ and $t_{\boldsymbol{r}\boldsymbol{r}\pm\hat{y}} = te^{\pm 2\pi i x/N_xN_y}$ under the Landau gauge used in [74,75].

Notice that the meaning of the Hamiltonian (23) is different depending on whether we regard it as a model of a chiral p-wave SC or as one of a chiral p-wave SC/QH insulator heterostructure. For the former case, c is the electron annihilation operator of the SC, and $\Delta_{\boldsymbol{r}\boldsymbol{r}+\boldsymbol{\delta}}$ is the mean field of the BCS theory assuming p-wave pairing. For the latter case, c is that of the QH insulator, and $\Delta_{\boldsymbol{r}\boldsymbol{r}+\boldsymbol{\delta}}$ is the pair potential induced in the QH insulator by the proximity effect from the chiral p-wave SC. Notice also that even for the chiral p-wave SC, one needs to incorporate the magnetic field via the Peierls phase [74,75]. As a result, it is reasonable to consider the same Hamiltonian for both systems, while the difference is the energy scale of μ and $\Delta_{\boldsymbol{r}\boldsymbol{r}+\boldsymbol{\delta}}$ compared with the hopping amplitude t, as will be specified later. Without the pair

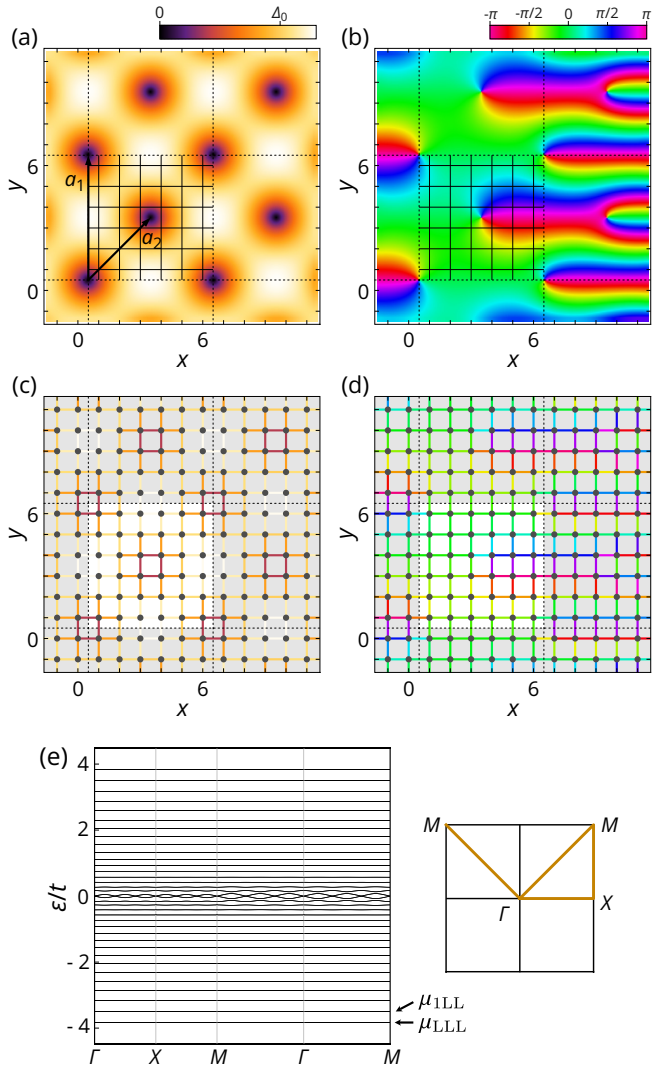

FIG. 2. (a) The absolute value and (b) the phase of the pair potential in the continuous space. Dashed lines represent the boundaries of a magnetic unit cell, and solid lines in a cell represent the lattice of the tight-binding model ($N_x = N_y = 6$). (c) and (d) represent the absolute value and the phase of the pair potential, respectively, assigned to the nearest-neighbor bonds in the tight-binding model. The outside of a magnetic unit cell is shaded. Colors of bonds are represented in a common scale with the corresponding continuous ones. (e) Electronic band structure without pair potentials. The horizontal axis is along a line shown in the Brillouin zone. The lowest and the second-lowest energy bands correspond to the lowest and first Landau levels (LLL and 1LL) whose energy is denoted by $\mu_{\rm LLL}$ and $\mu_{\rm 1LL}$, respectively.

potential, the model (23) shows a quantum Hall state where first few lowest energy bands are almost flat and have BdG Chern number 2 [Fig. 2(e)]. So, we call them the Landau levels.

We consider a pair potential forming a square vortex lattice whose lattice vectors are $\boldsymbol{a}_1 = (0, N_y)$ and $\boldsymbol{a}_2 = (N_x/2, N_y/2)$ [Figs. 2(a) and 2(b)]. The continuous pair potential on a cylinder is rescaled to fit the tight-binding model and is shifted so that the vortex position is $(1/2, 1/2)$ and $((N_x+1)/2, (N_y+1)/2)$ to avoid singularity on the lattice sites and bonds. The resulting pair potential is given by (see Appendix C)

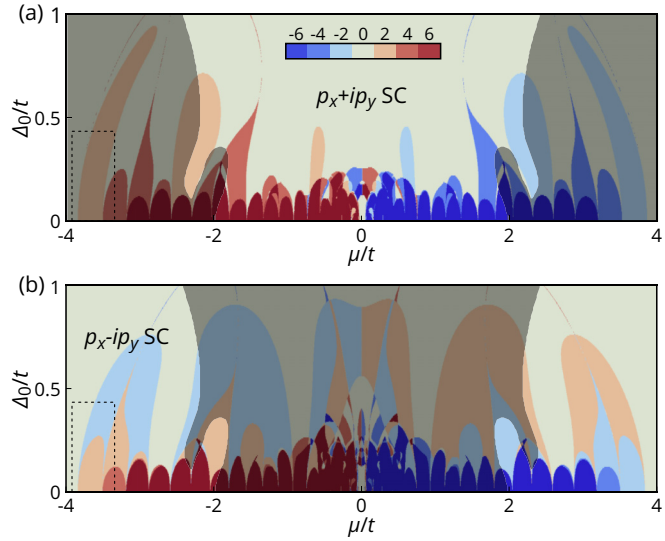

FIG. 3. The Bogoliubov-de Gennes (BdG) Chern number of mixed-state (a) $p_x + ip_y$-wave and (b) $p_x - ip_y$-wave superconductors. Phases with BdG Chern number larger than 6 or less than –6 are filled with the same colors for simplicity. Unshaded regions show that the corresponding chirality is energetically favored.

$$\Delta(\boldsymbol{r}) = \Delta_0 \sum_j e^{\pi i j^2/2} \exp\left[2\pi i j \frac{y - O_y}{N_y}\right] \times \exp\left[-2\pi \frac{(x - O_x + jN_x/2)^2}{N_x N_y}\right], \tag{24}$$

where $\boldsymbol{O} = (N_x/4 + 1/2, 3N_y/4 + 1/2)$ [Figs. 2(c) and 2(d)].

The Hamiltonian at this moment is not invariant under translation by $\boldsymbol{a}_2$. The translation invariance is recovered by introducing a singular gauge transformation [76]

$$c_{\boldsymbol{r}} \to e^{i\arg\Delta(\boldsymbol{r})/2} c_{\boldsymbol{r}}. \tag{25}$$

Since $\Delta(\boldsymbol{r} + \boldsymbol{a}_2) = e^{i\pi/2 - 2\pi i y/N_y}\Delta(\boldsymbol{r})$ and $t_{\boldsymbol{r}+2\boldsymbol{a}_2,\boldsymbol{r}+2\boldsymbol{a}_2\pm\hat{\boldsymbol{y}}} = t_{\boldsymbol{r},\boldsymbol{r}\pm\hat{\boldsymbol{y}}} e^{\pm 2\pi i/N_y}$ the translation invariance of the hopping amplitude is recovered. Notice that the singular gauge transformation (25) has a branch cut, so we introduce a branch cut line connecting neighboring two vortices [74] so that branch cut lines do not cross the boundaries of the magnetic unit cells. In the following, we consider $N_x = N_y = 6$ as shown in Figs. 2(a)–2(d).

The energy scale of the chemical potential μ and the pair potential Δ_0 for the chiral p-wave SC and the chiral p-wave SC/QH insulator heterostructure are determined as follows. For the chiral p-wave SC, we can consider arbitrary μ and Δ as long as the corresponding chirality is energetically favored (Fig. 3) and Δ_0 is sufficiently larger than that required for Δ_0 in the heterostructure. On the other hand, for the chiral p-wave SC/QH insulator heterostructure, we consider μ around the lowest and first Landau level ($\mu \sim \mu_{\rm LLL}, \mu_{\rm 1LL}$), and Δ_0 smaller than the Landau level spacing $\mu_{\rm 1LL} - \mu_{\rm LLL}$ (regions enclosed by dashed lines in Fig. 3).

B. Mixed-state chiral *p*-wave SC

The BdG Chern number of the mixed-state chiral p-wave SC in [74,75] has been evaluated far below H_{c2} as we mentioned in Sec. III D. Since a strong magnetic field is necessary for the integer and fractional QH effects, we examine whether the BdG Chern number of the mixed-state chiral p-wave SC is still even, even if the magnetic field is close to H_{c2}.

We numerically evaluate the BdG Chern number of mixed-state chiral p-wave SC close to H_{c2} by (23) with (24) [Figs. 3(a) and 3(b)]. The BdG Chern number is always even irrespective of the magnitude of Δ_0 and μ. Notice that the BdG Chern number of the chiral p-wave SC without the vortex lattice is ± 1 when $\mathrm{sgn}[C\mu] \lessgtr 0$, where C is the chirality of the pair potential. The energetically favored pairing chirality is shown by unshaded regions in Fig. 3. This indicates that the chirality can be tuned by the chemical potential. Notice that the phase diagram around the $(n+1)$th Landau level of the $p_x + ip_y$-wave SC and that around the nth Landau level of the $p_x - ip_y$-wave SC have a similar structure within a small Δ, albeit the difference of the BdG Chern number by 2. This can be understood by an identity

$$\Delta^{p_x - ip_y}_{nknk'} = \Delta^{p_x + ip_y}_{n+1kn+1k'} \tag{26}$$

of the continuum model from (B9).

C. Mixed-state chiral *p*-wave SC/QH insulator

Since we confirmed that the mixed-state chiral p-wave SC has even BdG Chern number $\mathcal{N}$, its heterostructure with a QH insulator can have odd $\mathcal{N}$ phases when a topological phase transition occurs. We will see that only the $p_x - ip_y$-wave pair potential can give rise to such a topological phase transition in the LLL.

We consider a QH insulator coupled with the proximity effect from a mixed-state chiral p-wave SC given by (23) with (24). In particular, we focus on μ close to the LLL (μ_{LLL}) and the first Landau level ($\mu_{1\mathrm{LL}}$), and Δ smaller than $\mu_{1\mathrm{LL}} - \mu_{\mathrm{LLL}}$. Let the momentum-space BdG Hamiltonian of (23) be denoted by $h(\boldsymbol{k})$. The eigenenergies of $h(\boldsymbol{k})$ when $\mu = \mu_{\mathrm{LLL}}$ are shown in Fig. 4(a) (left). By diagonalizing the electron and hole parts of $h(\boldsymbol{k})$ separately, we obtain

$$h(\boldsymbol{k}) = \begin{pmatrix} h_0(\boldsymbol{k}) & \Delta(\boldsymbol{k}) \\ \Delta^\dagger(\boldsymbol{k}) & -h_0^*(-\boldsymbol{k}) \end{pmatrix} \rightarrow \begin{pmatrix} \mathrm{diag}[\epsilon_0(\boldsymbol{k}) - \mu, \ldots] & \tilde{\Delta}(\boldsymbol{k}) \\ \tilde{\Delta}^\dagger(\boldsymbol{k}) & \mathrm{diag}[-\epsilon_0(-\boldsymbol{k}) + \mu, \ldots] \end{pmatrix}, \tag{27}$$

where $\epsilon_0(\boldsymbol{k})$ is the LLL energy. The (1,1)-component of $\tilde{\Delta}(\boldsymbol{k})$ in (27) is shown in Fig. 4(a) (center and right). This quantity is the expectation value of the pair potential with respect to the LLL, and is the lattice counterpart of (16) with $n = n' = 0$. The energy band remains flat under the $p_x + ip_y$-wave pair potential, and the expectation value of the $p_x + ip_y$-wave pair potential is two orders of magnitude smaller than that of the $p_x - ip_y$-wave one. These features cannot be seen in the first Landau level ($\mu = \mu_{1\mathrm{LL}}$) [Fig. 4(b)]. Notice that the coincidence of the $p_x - ip_y$-wave pair potential on the LLL and the $p_x + ip_y$-wave pair potential on the first Landau level [Figs. 4(a) (right) and 4(b) (center)] agrees with (26). It is interesting to observe the quasiparticle energy spectra are also similar for $p_x - ip_y$ at the LLL and for $p_x + ip_y$ at the first Landau level [red curves in Fig. 4(a) (left) and black curves in Fig. 4(b) (left)].

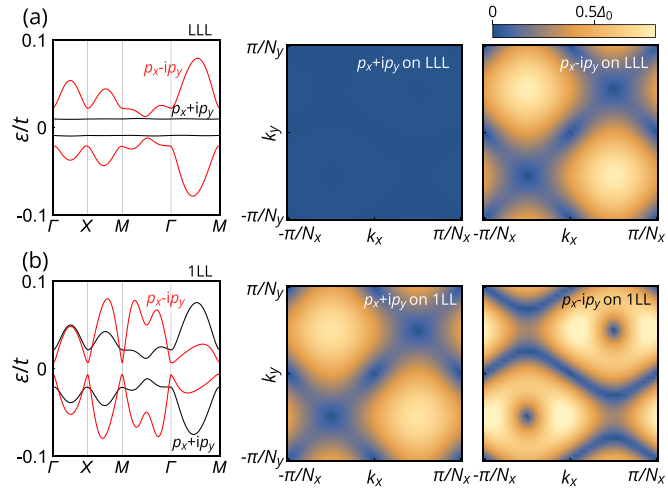

FIG. 4. (a) Quasiparticle energy spectra with $p_x \pm ip_y$-wave pair potential (24) with $\Delta_0 = 0.1$ at μ_{LLL}. The center and right figures are the expectation value of the pair potential with respect to the LLL states in the Brillouin zone. (b) The same plots as (a) at $\mu_{1\mathrm{LL}}$.

We numerically evaluate the BdG Chern number $\mathcal{N}$ of this system. Here, we set μ to be around the lowest and first Landau level, and Δ to be up to the order of the energy gap between the two bands ($\sim 0.3t$) [which shares the same phase diagram as the chiral p-wave SC surrounded by dashed lines in Figs. 3(a) and 3(b)]. Notice that the chemical potential μ of the QH insulator is irrelevant to that of the attached chiral p-wave SC in the previous subsection, while the pair potential Δ induced in the QH insulator is assumed to be proportional to that of the chiral p-wave SC. The energy gap and the BdG Chern number $\mathcal{N}$ are shown in Figs. 5(a) and 5(b) for $p_x \pm ip_y$-wave, respectively. The appearance of the phase with $\mathcal{N} = -2$ is a result of the proximity effect from the mixed-state $p_x - ip_y$-wave SC, while no new phases other than $\mathcal{N} = 0$ and 2 appear for the $p_x + ip_y$-wave case since the proximity effect does not work on the LLL.

We can generate odd $\mathcal{N}$ phases between even $\mathcal{N}$ phases by adding external potentials [69]. A topological phase transition accompanying more than $\mathcal{N} = 1$ change can be split into those accompanying $\mathcal{N} = 1$ change. Specifically, for a topological phase transition from $\mathcal{N} = 2$ to -2 in Fig. 5(b) around $\delta\mu/t \equiv (\mu - \mu_{\mathrm{LLL}})/t \sim 0.2$, there are four momenta $\boldsymbol{k} = (0,0), (0,\pi/N_y), (\pi/N_x, 0), (\pi/N_x, \pi/N_y)$ where the gap closes (Fig. 4). A potential

$$V(\boldsymbol{k}) = V_x \cos k_x N_x + V_y \cos k_y N_y \tag{28}$$

with $V_x \neq V_y$ shifts the chemical potential at the four momenta differently. As a result, topological phase transitions occur one by one by changing the chemical potential.

The phase diagrams with $V_x = 0.01$ and $V_y = 0.02$ are shown in Figs. 5(c) and 5(d) for $p_x \pm ip_y$-wave,

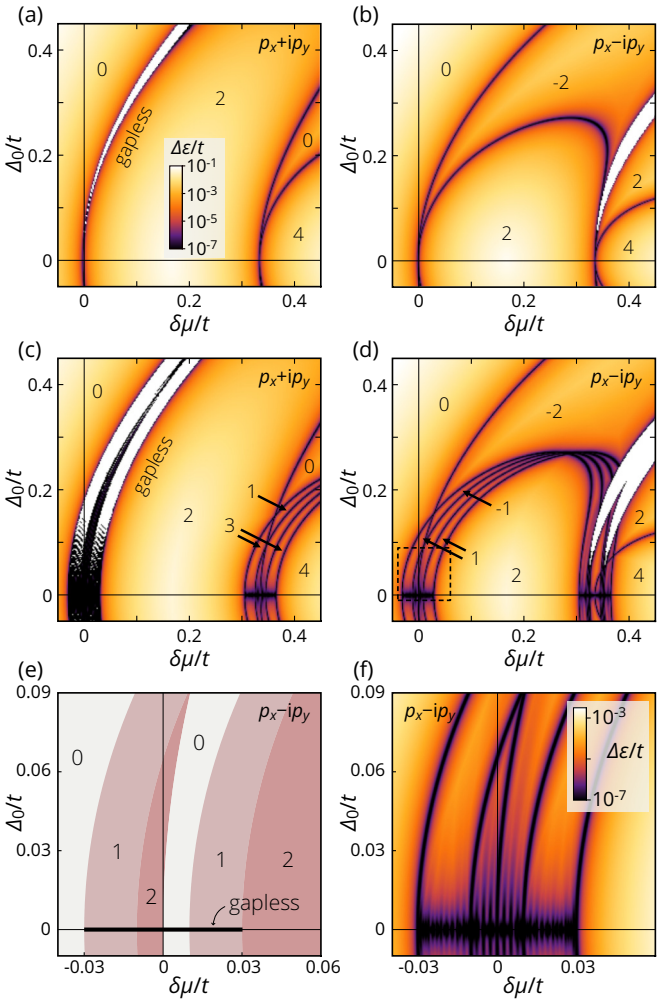

FIG. 5. The phase diagrams of a quantum Hall insulator proximity-coupled with a $p_x + ip_y$- (a), (c) and $p_x - ip_y$-wave (b), (d) superconductor without (a), (b) and with (c), (d) a potential (28) with $V_x = 0.01$ and $V_y = 0.02$. Color indicates the indirect energy gap $\Delta\epsilon$. $\delta\mu$ is the chemical potential measured from the lowest Landau level energy. The numbers inside the figures stands for the Bogoliubov-de Gennes Chern number. The indirect band gap vanishes in white regions, that is, the lowest Bogoliubov quasi-particle band bents below the zero energy. (e) and (f) are the phase diagram and the energy gap, respectively, of the region shown by a dashed line in (d).

respectively. By the $p_x + ip_y$-wave pair potential, the LLL becomes dispersive but never becomes a topological SC. On the other hand, topological SC phases appear near the first Landau level. By the $p_x - ip_y$-wave pair potential, topological SC phases appear even near the LLL. These results agree with the prediction by the continuum model in the previous section. The detailed phase diagram and the energy gap for the $p_x - ip_y$-wave case is shown in Figs. 5(e) and 5(f). We can turn the LLL states into a topological SC by an infinitesimally small pair potential.

V. CONCLUSIONS

In this study, we consider SC/QH heterostructures and elucidate the role played by the vortex lattice in pairing bulk quantum Hall states. Although the necessity of the vortex lattice was suggested even from the consideration of practical SC/QH heterostructures in Sec. II A, it turned out to be essential in inducing the bulk proximity effect irrespective of pairing symmetry. By using the disk geometry, we showed that Cooper pairs with finite angular momenta generated by the vortex lattice can make pairs between time-reversal-symmetry broken states in the bulk QH state. What we believe is essential in this conclusion is that we need to incorporate a magnetic field properly even in the SC side when we consider SC/QH heterostructures. In this sense, it would be interesting to extend our result to a magnetic field away from H_{c2}, where the superconducting flux quantum is distributed sparsely and hence the pair potential can no longer be written in terms of the LLL wavefunctions of Cooper pairs as in (11).

As an example, we considered a mixed-state chiral p-wave SC/QH insulator heterostructure, where both systems have distinct chiralities. The presence of a vortex lattice is not sufficient in pairing the LLL state; we need to align the relative chirality between the pairing and the quantum Hall states. The pair potential from the opposite chirality SC is blocked in the LLL, while that from the same chirality gives rise to a topological phase transition to a topological SC with the aid of an external potential. We confirmed these claims by both analytical calculations using a continuum model and numerical calculations using a tight-binding model.

Notice that we do not mean that our heterostructure is useful in constructing a topological superconductor, since we made a topological SC from another topological SC. We focus in particular on the physics underlying general SC/QH heterostructures rather than material science. We believe that our study paves the way for engineering heterostructures with more exotic materials hosting non-Abelian anyons.

Recently, the observation of the fractional quantum anomalous Hall effect in moiré materials such as twisted $MoTe_2$ bilayers [77–82] and rhombohedral multilayer graphene [83–87] has attracted particular attention. Heterostructures of these materials with SCs could realize SC/QH heterostructures without a magnetic field. Though the electronic state of some of these materials is still under active discussion, it would be interesting to study the condition for a valid proximity effect in moiré quantum anomalous Hall states.

ACKNOWLEDGMENTS

We thank Akira Furusaki, Masayuki Hashisaka, and Yukio Tanaka for discussions. The work is supported in part by JSPS KAKENHI Grants No. JP24K06926, No. JP23K19036, No. JP25K17318, No. JP25H01250, and No. JP25H00613.

DATA AVAILABILITY

The data that support the findings of this article are not publicly available upon publication because it is not technically feasible and/or the cost of preparing, depositing, and hosting the data would be prohibitive within the terms of this research project. The data are available from the authors upon reasonable request.

APPENDIX A: MATRIX ELEMENTS OF MIXED-STATE PAIR POTENTIALS

Here, we derive the matrix elements (12) and (20) of the mixed-state s-wave and $p_x - ip_y$-wave pair potentials, respectively. From (7) and (11), one obtains

$$\Delta^s_{nmn'm'} = \int d\boldsymbol{r}\phi^*_{nm}(\boldsymbol{r})\Delta(\boldsymbol{r})\phi^*_{n'm'}(\boldsymbol{r}) = \frac{(-1)^{n+n'}C_{m+m'}}{2\sqrt{\pi}\ell_B}\sqrt{\frac{n!n'!(m+m')!}{2^{m+m'}(n+m)!(n'+m')!}}I_{nmn'm'}, \tag{A1}$$

where

$$I_{nmn'm'} = \frac{2^{m+m'+1}}{(m+m')!}\int_0^\infty dx\, x^{m+m'}e^{-2x}L^m_n(x)L^{m'}_{n'}(x). \tag{A2}$$

Using $L^m_0(x) = 1$ and $L^m_1(x) = m + 1 - x$, one can readily calculate (A2) for the first few cases as

$$I_{0m0m'} = 1, \tag{A3}$$

$$I_{1m0m'} = \frac{m - m' + 1}{2}. \tag{A4}$$

Notice that $I_{0m1m'}$ can be obtained from (A4) by an identity $I_{nmn'm'} = I_{n'm'nm}$. These results are sufficient to evaluate (12) and (20) using the $n = n' = 0$ case of (18), that is,

$$\Delta^{p_x-ip_y}_{0m0m'} = -\frac{i\hbar}{2\sqrt{2}\ell_B}\left(\Delta^s_{1m-10m'} - \Delta^s_{0m1m'-1}\right). \tag{A5}$$

For arbitrary n and n', one obtains

$$I_{nmn'm'} = \sum_{j=0}^{n}\sum_{k=0}^{n'}\binom{n+m}{n-j}\binom{n'+m'}{n'-k}\frac{(m+m'+1)_{j+k}}{(-2)^{j+k}j!k!}, \tag{A6}$$

where $(a)_n = \Gamma(a+n)/\Gamma(a)$ is the Pochhammer symbol, by using an expression of the associated Laguerre polynomial

$$L^m_n(x) = \sum_{j=0}^{n}(-1)^j\binom{n+m}{n-j}\frac{x^j}{j!}. \tag{A7}$$

We anticipate that the absolute value of the coefficient C_m is approximately independent of m because of the following reason. The integral of the squared amplitude of the pair potential over a sufficiently large region S should be proportional to its area $|S|$ as the vortex lattice is uniformly distributed. From (B5),

$$\int_S d\boldsymbol{r}|\Delta(\boldsymbol{r})|^2 = \sum_{m\geqslant 0}|C_m|^2 \simeq \langle|\Delta(\boldsymbol{r})|^2\rangle|S|, \tag{A8}$$

where $\langle\cdots\rangle$ denotes the spatial average. Here, we consider a disk of radius $\sqrt{m_0}\ell_B$. Since each term in (11) is distributed around a circle of radius $\sqrt{m}\ell_B$, the upper bound of the summation of (A8) is approximately m_0 and its area is $|S| = \pi m_0\ell_B^2$. Since this approximate relation holds for any (sufficiently large) m_0, one can conclude that $|C_m| \simeq \ell_B\sqrt{\pi\langle|\Delta(\boldsymbol{r})|^2\rangle}$, which does not depend on m.

APPENDIX B: MIXED-STATE PAIR POTENTIAL ON A CYLINDER

We consider a continuum model of a mixed-state chiral p-wave SC/QH insulator heterostructure on a cylinder for comparison with a lattice model. This argument will be proceeded basically in parallel with the previous studies with mixed-state s-wave superconductors [69,70].

The QH state wavefunction on a cylinder that is periodic in the y direction with circumference L_y is given under the Landau gauge $\boldsymbol{A} = (0, Bx)$, by [73]

$$\phi_{nk}(\boldsymbol{r}) = \frac{(a^\dagger_k)^n}{\sqrt{n!}}\phi_{0k}(\boldsymbol{r}) = \frac{e^{iky}}{\sqrt{L_y}}\frac{1}{\sqrt{2^n n!\ell_B\sqrt{\pi}}}e^{-(x-x_k)^2/2\ell_B^2}H_n\left(\frac{x-x_k}{\ell_B}\right), \tag{B1}$$

where $n \in \mathbb{Z}_{\geqslant 0}$, $k = 2\pi j/L_y\,(j \in \mathbb{Z})$, $a_k = [\ell_B\partial_x + (x - x_k)/\ell_B]/\sqrt{2}$, $x_k = -k\ell_B^2$, and H_n is the Hermite polynomial. The s-wave and chiral p-wave pairing Hamiltonians are given by (2) and (14), respectively. The s-wave pairing Hamiltonian on the basis of (B1) is given by

$$H^s_\Delta = \sum_{nkn'k'}\Delta^s_{nkn'k'}c^\dagger_{nk\uparrow}c^\dagger_{n'k'\downarrow} + \text{H.c.}, \tag{B2}$$

where

$$\Delta^s_{nkn'k'} = \int d\boldsymbol{r}\phi^*_{nk}(\boldsymbol{r})\Delta(\boldsymbol{r})\phi^*_{n'k'}(\boldsymbol{r}). \tag{B3}$$

Notice that if the s-wave pair potential is uniform [$\Delta(\boldsymbol{r}) = \Delta_0$], the pair potential is nonzero only when $k' = -k$ and is given by

$$\Delta^s_{nkn'-k} = \Delta_0\sqrt{\frac{2^{n'}n!}{2^n n'!}}e^{-x_k^2/\ell_B^2}\left(\frac{x_k}{\ell_B}\right)^{n'-n}L^{n'-n}_n\left(\frac{2x_k^2}{\ell_B^2}\right), \tag{B4}$$

where L^α_n is the associated Laguerre polynomial. Unlike the disk case, the number of induced pairs are not limited by a constant. The strongest pairing is that between $k = 0$ states, where $x_k = x_{-k} = 0$ and are related by the time-reversal operation. However, the matrix element decays exponentially as x_k is far away from $x = 0$. In this sense, the same conclusion as in the disk case holds, that is, a uniform s-wave pair potential does not induce an extensive number of Cooper pairs in QH states.

The induced pair potential $\Delta(\boldsymbol{r})$ close to H_{c2} is spanned by the LLL wavefunctions of Cooper pairs as [72]

$$\Delta(\boldsymbol{r}) = \sum_{j\in\mathbb{Z}}C_j e^{iq_j y}e^{-(x-\tilde{x}_{q_j})^2/\ell_B^2}, \tag{B5}$$

where $\tilde{x}_q = -q\ell_B^2/2$. When the lattice vectors of the vortex lattice are $\boldsymbol{a}_1 = (0, \Delta y)$ and $\boldsymbol{a}_2 = (\Delta x, \Delta y\sin\theta)$, the momentum is given by $q_j = 2\pi j/\Delta y\,(j \in \mathbb{Z})$. The resulting matrix element of (B5) is given by [69,70]

$$\Delta^s_{nkn'k} = \sum_j\frac{(-1)^n C_j\delta_{q_j,k+k'}}{2^{n+n'}\sqrt{2n!n'!}}e^{-(x_k-x_{k'})^2/4\ell_B^2}H_{n+n'}\left(\frac{x_k - x_{k'}}{\sqrt{2}\ell_B}\right). \tag{B6}$$

As in the disk geometry, the matrix elements of chiral p-wave pair potentials defined by

$$H_{\Delta}^{p_x\pm ip_y} = \sum_{nkn'k'} \Delta_{nkn'k'}^{p_x\pm ip_y} c_{nk}^{\dagger} c_{n'k'}^{\dagger} + \text{H.c.} \tag{B7}$$

are related to those of the s-wave one provided they share the same $\Delta(\boldsymbol{r})$. Since the covariant derivative for electronic Landau level states of momentum k is given by

$$e^{-iky}(-i\hbar D_{\pm}^{e})e^{iky} = \frac{\sqrt{2}i\hbar}{\ell_B}\begin{cases} a_k^{\dagger} & (+) \\ -a_k & (-) \end{cases}, \tag{B8}$$

we obtain

$$\begin{aligned} &\Delta_{nkn'k'}^{p_x\pm ip_y} \\ &\equiv \frac{1}{2}\int d\boldsymbol{r}\psi_{nk}^{*}\frac{-i\hbar D_{\pm}^{h}\Delta + \Delta(-i\hbar D_{\pm}^{e})}{2}\psi_{n'k'}^{*} = -\frac{i\hbar}{2\sqrt{2}\ell_B} \\ &\times \begin{cases} -\sqrt{n}\Delta_{n-1kn'k'}^{s} + \sqrt{n'}\Delta_{nkn'-1k'}^{s} & (p_x+ip_y) \\ \sqrt{n+1}\Delta_{n+1kn'k'}^{s} - \sqrt{n'+1}\Delta_{nkn'+1k'}^{s} & (p_x-ip_y) \end{cases}. \end{aligned} \tag{B9}$$

Projecting onto the LLL ($n = n' = 0$) and assuming (B5), the pair potential is zero for the $p_x + ip_y$ wave while for the $p_x - ip_y$ wave,

$$\Delta_{0k0k'}^{p_x-ip_y} = -\frac{i\hbar}{\sqrt{2}\ell_B}\Delta_{1k0k'}^{s}. \tag{B10}$$

Equation (B10) is the same form as the one in a heterostructure of a mixed-state s-wave SC and a Rashba-coupled QH insulator [69,70]. A similar calculation on a sphere could also be done following [71].

APPENDIX C: PAIR POTENTIAL IN THE TIGHT-BINDING MODEL

The coefficients C_j in (B5) are determined by imposing the periodicity of the vortex lattice. Two lattice vectors of the vortex lattice are denoted by $\boldsymbol{a}_1 = (0, \Delta y)$ and $\boldsymbol{a}_2 = (\Delta x, \Delta y \sin\theta)$. Notice that as two superconducting fluxes is equal to a flux quantum h/e, Δx and Δy are related by $\Delta x \Delta y = \pi \ell_B^2$ that is half of the area occupied by a flux quantum. From $\boldsymbol{a}_1$, the momentum is given by $q_j = 2\pi j/\Delta y$ ($j \in \mathbb{Z}$). The coefficient is given by $C_j = \Delta_0 \exp[i\pi j^2 \cos\theta]$ [72], that is,

$$\Delta(\boldsymbol{r}) = \Delta_0 \sum_{j\in\mathbb{Z}} e^{i\pi j^2\cos\theta} e^{2\pi ijy/\Delta y} e^{-\pi(x+j\Delta x)^2/\Delta x\Delta y}. \tag{C1}$$

Notice that the position of the vortices is $(\boldsymbol{a_1} + \boldsymbol{a_2})/2$ and their translations by $\boldsymbol{a}_1$ and $\boldsymbol{a}_2$.

A mixed-state pair potential on a square lattice model in Sec. IV is given by rescaling (C1). Specifically, we consider an $N_x \times N_y$ magnetic unit cell in unit of the lattice constant of the tight-binding model, which contains two superconducting fluxes at the corners and the center of it [see Fig. 2(a)]. This gives $2\Delta x = N_x$, $\Delta y = N_y$, and $\cos\theta = 1/2$. Moreover, we translate the origin to $\boldsymbol{O}$ so that vortices in a magnetic unit cell are at $(1/2, 1/2)$ and $((N_x+1)/2, (N_y+1)/2)$. This leads to an equation

$$\left(\frac{1}{2}, \frac{1}{2}\right) = \boldsymbol{O} - \frac{\boldsymbol{a_1} + \boldsymbol{a_2}}{2}. \tag{C2}$$

From these result, we obtain (24).

[1] D. A. Ivanov, Non-Abelian statistics of half-quantum vortices in p-wave superconductors, Phys. Rev. Lett. **86**, 268 (2001).

[2] J. Alicea, New directions in the pursuit of Majorana fermions in solid state systems, Rep. Prog. Phys. **75**, 076501 (2012).

[3] C. Beenakker, Search for Majorana fermions in superconductors, Annu. Rev. Condens. Matter Phys. **4**, 113 (2013).

[4] G. E. Volovik, *The Universe in a Helium Droplet* (Oxford University Press, Oxford, 2009).

[5] G. Moore and N. Read, Nonabelions in the fractional quantum Hall effect, Nucl. Phys. B **360**, 362 (1991).

[6] X. G. Wen, Non-Abelian statistics in the fractional quantum Hall states, Phys. Rev. Lett. **66**, 802 (1991).

[7] N. Read and D. Green, Paired states of fermions in two dimensions with breaking of parity and time-reversal symmetries and the fractional quantum Hall effect, Phys. Rev. B **61**, 10267 (2000).

[8] A. Y. Kitaev, Unpaired Majorana fermions in quantum wires, Phys. Usp. **44**, 131 (2001).

[9] A. Kitaev, Anyons in an exactly solved model and beyond, Ann. Phys. **321**, 2 (2006).

[10] J. K. Jain, Composite-fermion approach for the fractional quantum Hall effect, Phys. Rev. Lett. **63**, 199 (1989).

[11] L. Fu and C. L. Kane, Superconducting proximity effect and Majorana fermions at the surface of a topological insulator, Phys. Rev. Lett. **100**, 096407 (2008).

[12] A. R. Akhmerov, J. Nilsson, and C. W. J. Beenakker, Electrically detected interferometry of Majorana fermions in a topological insulator, Phys. Rev. Lett. **102**, 216404 (2009).

[13] L. Fu and C. L. Kane, Josephson current and noise at a superconductor/quantum-spin-Hall-insulator/superconductor junction, Phys. Rev. B **79**, 161408(R) (2009).

[14] X.-L. Qi, T. L. Hughes, and S.-C. Zhang, Chiral topological superconductor from the quantum Hall state, Phys. Rev. B **82**, 184516 (2010).

[15] J. D. Sau, R. M. Lutchyn, S. Tewari, and S. Das Sarma, Generic new platform for topological quantum computation using semiconductor heterostructures, Phys. Rev. Lett. **104**, 040502 (2010).

[16] R. M. Lutchyn, J. D. Sau, and S. Das Sarma, Majorana fermions and a topological phase transition in semiconductor-superconductor heterostructures, Phys. Rev. Lett. **105**, 077001 (2010).

[17] Y. Oreg, G. Refael, and F. von Oppen, Helical liquids and Majorana bound states in quantum wires, Phys. Rev. Lett. **105**, 177002 (2010).

[18] V. Mourik, K. Zuo, S. M. Frolov, S. R. Plissard, E. P. A. M. Bakkers, and L. P. Kouwenhoven, Signatures of Majorana fermions in hybrid superconductor-semiconductor nanowire devices, Science **336**, 1003 (2012).

[19] T.-P. Choy, J. M. Edge, A. R. Akhmerov, and C. W. J. Beenakker, Majorana fermions emerging from magnetic nanoparticles on a superconductor without spin-orbit coupling, Phys. Rev. B **84**, 195442 (2011).

[20] S. Nadj-Perge, I. K. Drozdov, B. A. Bernevig, and A. Yazdani, Proposal for realizing majorana fermions in chains of magnetic atoms on a superconductor, Phys. Rev. B **88**, 020407(R) (2013).

[21] B. Braunecker and P. Simon, Interplay between classical magnetic moments and superconductivity in quantum one-dimensional conductors: Toward a self-sustained topological Majorana phase, Phys. Rev. Lett. **111**, 147202 (2013).

[22] J. Klinovaja, P. Stano, A. Yazdani, and D. Loss, Topological superconductivity and Majorana fermions in RKKY systems, Phys. Rev. Lett. **111**, 186805 (2013).

[23] M. M. Vazifeh and M. Franz, Self-organized topological state with Majorana fermions, Phys. Rev. Lett. **111**, 206802 (2013).

[24] F. Pientka, L. I. Glazman, and F. von Oppen, Topological superconducting phase in helical Shiba chains, Phys. Rev. B **88**, 155420 (2013).

[25] S. Nakosai, Y. Tanaka, and N. Nagaosa, Two-dimensional p-wave superconducting states with magnetic moments on a conventional s-wave superconductor, Phys. Rev. B **88**, 180503(R) (2013).

[26] S. Nadj-Perge, I. K. Drozdov, J. Li, H. Chen, S. Jeon, J. Seo, A. H. MacDonald, B. A. Bernevig, and A. Yazdani, Observation of Majorana fermions in ferromagnetic atomic chains on a superconductor, Science **346**, 602 (2014).

[27] F. S. Bergeret, A. F. Volkov, and K. B. Efetov, Long-range proximity effects in superconductor-ferromagnet structures, Phys. Rev. Lett. **86**, 4096 (2001).

[28] F. S. Bergeret, A. F. Volkov, and K. B. Efetov, Odd triplet superconductivity and related phenomena in superconductor-ferromagnet structures, Rev. Mod. Phys. **77**, 1321 (2005).

[29] M. Eschrig, T. Löfwander, T. Champel, J. C. Cuevas, J. Kopu, and G. Schön, Symmetries of pairing correlations in superconductor–ferromagnet nanostructures, J. Low Temp. Phys. **147**, 457 (2007).

[30] N. Bovenzi, M. Breitkreiz, P. Baireuther, T. E. O'Brien, J. Tworzydło, i. d. I. Adagideli, and C. W. J. Beenakker, Chirality blockade of Andreev reflection in a magnetic Weyl semimetal, Phys. Rev. B **96**, 035437 (2017).

[31] N. H. Lindner, E. Berg, G. Refael, and A. Stern, Fractionalizing majorana fermions: Non-Abelian statistics on the edges of Abelian quantum Hall states, Phys. Rev. X **2**, 041002 (2012).

[32] D. J. Clarke, J. Alicea, and K. Shtengel, Exotic non-Abelian anyons from conventional fractional quantum Hall states, Nat. Commun. **4**, 1348 (2013).

[33] R. S. K. Mong, D. J. Clarke, J. Alicea, N. H. Lindner, P. Fendley, C. Nayak, Y. Oreg, A. Stern, E. Berg, K. Shtengel, and M. P. A. Fisher, Universal topological quantum computation from a superconductor-Abelian quantum Hall heterostructure, Phys. Rev. X **4**, 011036 (2014).

[34] A. Vaezi, Superconducting analog of the parafermion fractional quantum Hall states, Phys. Rev. X **4**, 031009 (2014).

[35] M. Ma and A. Y. Zyuzin, Josephson effect in the quantum Hall regime, Europhys. Lett. **21**, 941 (1993).

[36] A. Y. Zyuzin, Superconductor–normal-metal–superconductor junction in a strong magnetic field, Phys. Rev. B **50**, 323 (1994).

[37] M. P. A. Fisher, Cooper-pair tunneling into a quantum Hall fluid, Phys. Rev. B **49**, 14550 (1994).

[38] D. L. Maslov, M. Stone, P. M. Goldbart, and D. Loss, Josephson current and proximity effect in Luttinger liquids, Phys. Rev. B **53**, 1548 (1996).

[39] Y. Ishikawa and H. Fukuyama, Effects of magnetic field on Josephson current in SNS system, J. Phys. Soc. Jpn. **68**, 954 (1999).

[40] F. Giazotto, M. Governale, U. Zülicke, and F. Beltram, Andreev reflection and cyclotron motion at superconductor–normal-metal interfaces, Phys. Rev. B **72**, 054518 (2005).

[41] M. Stone and Y. Lin, Josephson currents in quantum Hall devices, Phys. Rev. B **83**, 224501 (2011).

[42] B. Lian, J. Wang, and S.-C. Zhang, Edge-state-induced Andreev oscillation in quantum anomalous Hall insulator-superconductor junctions, Phys. Rev. B **93**, 161401(R) (2016).

[43] Z. Hou, Y. Xing, A.-M. Guo, and Q.-F. Sun, Crossed Andreev effects in two-dimensional quantum Hall systems, Phys. Rev. B **94**, 064516 (2016).

[44] L. Cohnitz, A. De Martino, W. Häusler, and R. Egger, Proximity-induced superconductivity in Landau-quantized graphene monolayers, Phys. Rev. B **96**, 140506(R) (2017).

[45] O. Gamayun, J. A. Hutasoit, and V. V. Cheianov, Two-terminal transport along a proximity-induced superconducting quantum Hall edge, Phys. Rev. B **96**, 241104(R) (2017).

[46] R. Nakai, K. Nomura, and Y. Tanaka, Edge-induced pairing states in a Josephson junction through a spin-polarized quantum anomalous Hall insulator, Phys. Rev. B **103**, 184509 (2021).

[47] L. Peralta Gavensky, G. Usaj, and C. A. Balseiro, Imaging chiral Andreev reflection in the presence of Rashba spin-orbit coupling, Phys. Rev. B **104**, 115435 (2021).

[48] A. L. R. Manesco, I. M. Flór, C.-X. Liu, and A. R. Akhmerov, Mechanisms of Andreev reflection in quantum Hall graphene, SciPost Phys. Core **5**, 045 (2022).

[49] Y. Tang, C. Knapp, and J. Alicea, Vortex-enabled Andreev processes in quantum Hall–superconductor hybrids, Phys. Rev. B **106**, 245411 (2022).

[50] A. David, J. S. Meyer, and M. Houzet, Geometrical effects on the downstream conductance in quantum-Hall–superconductor hybrid systems, Phys. Rev. B **107**, 125416 (2023).

[51] V. D. Kurilovich and L. I. Glazman, Criticality in the crossed Andreev reflection of a quantum Hall edge, Phys. Rev. X **13**, 031027 (2023).

[52] V. D. Kurilovich, Z. M. Raines, and L. I. Glazman, Disorder-enabled Andreev reflection of a quantum Hall edge, Nat. Commun. **14**, 2237 (2023).

[53] A. B. Michelsen, P. Recher, B. Braunecker, and T. L. Schmidt, Supercurrent-enabled Andreev reflection in a chiral quantum Hall edge state, Phys. Rev. Res. **5**, 013066 (2023).

[54] L. Arrachea, A. L. Yeyati, and C. A. Balseiro, Signatures of triplet superconductivity in $\nu = 2$ chiral Andreev states, Phys. Rev. B **109**, 064519 (2024).

[55] F. Amet, C. T. Ke, I. V. Borzenets, J. Wang, K. Watanabe, T. Taniguchi, R. S. Deacon, M. Yamamoto, Y. Bomze, S. Tarucha, and G. Finkelstein, Supercurrent in the quantum Hall regime, Science **352**, 966 (2016).

[56] G.-H. Lee, K.-F. Huang, D. K. Efetov, D. S. Wei, S. Hart, T. Taniguchi, K. Watanabe, A. Yacoby, and P. Kim, Inducing superconducting correlation in quantum Hall edge states, Nat. Phys. **13**, 693 (2017).

[57] G.-H. Park, M. Kim, K. Watanabe, T. Taniguchi, and H.-J. Lee, Propagation of superconducting coherence via chiral quantum-Hall edge channels, Sci. Rep. **7**, 10953 (2017).

[58] A. Seredinski, A. W. Draelos, E. G. Arnault, M.-T. Wei, H. Li, T. Fleming, K. Watanabe, T. Taniguchi, F. Amet, and G. Finkelstein, Quantum Hall–based superconducting interference device, Sci. Adv. **5**, eaaw8693 (2019).

[59] L. Zhao, E. G. Arnault, A. Bondarev, A. Seredinski, T. F. Q. Larson, A. W. Draelos, H. Li, K. Watanabe, T. Taniguchi, F. Amet, H. U. Baranger, and G. Finkelstein, Interference of chiral Andreev edge states, Nat. Phys. **16**, 862 (2020).

[60] M. Hatefipour, J. J. Cuozzo, J. Kanter, W. M. Strickland, C. R. Allemang, T.-M. Lu, E. Rossi, and J. Shabani, Induced superconducting pairing in integer quantum Hall edge states, Nano Lett. **22**, 6173 (2022).

[61] H. Vignaud, D. Perconte, W. Yang, B. Kousar, E. Wagner, F. Gay, K. Watanabe, T. Taniguchi, H. Courtois, Z. Han, H. Sellier, and B. Sacépé, Evidence for chiral supercurrent in quantum Hall Josephson junctions, Nature (London) **624**, 545 (2023).

[62] J. Barrier, M. Kim, R. K. Kumar, N. Xin, P. Kumaravadivel, L. Hague, E. Nguyen, A. I. Berdyugin, C. Moulsdale, V. V. Enaldiev *et al.*, One-dimensional proximity superconductivity in the quantum Hall regime, Nature (London) **628**, 741 (2024).

[63] O. Gül, Y. Ronen, S. Y. Lee, H. Shapourian, J. Zauberman, Y. H. Lee, K. Watanabe, T. Taniguchi, A. Vishwanath, A. Yacoby, and P. Kim, Andreev reflection in the fractional quantum Hall state, Phys. Rev. X **12**, 021057 (2022).

[64] I. E. Nielsen, K. Flensberg, R. Egger, and M. Burrello, Readout of parafermionic states by transport measurements, Phys. Rev. Lett. **129**, 037703 (2022).

[65] N. Schiller, B. A. Katzir, A. Stern, E. Berg, N. H. Lindner, and Y. Oreg, Superconductivity and fermionic dissipation in quantum Hall edges, Phys. Rev. B **107**, L161105 (2023).

[66] G. S. Jeon, J. K. Jain, and C.-X. Liu, Topological superconductivity in Landau levels, Phys. Rev. B **99**, 094509 (2019).

[67] J. Schirmer, C.-X. Liu, and J. K. Jain, Phase diagram of superconductivity in the integer quantum Hall regime, Proc. Natl. Acad. Sci. USA **119**, e2202948119 (2022).

[68] B. Zocher and B. Rosenow, Topological superconductivity in quantum Hall–superconductor hybrid systems, Phys. Rev. B **93**, 214504 (2016).

[69] R. V. Mishmash, A. Yazdani, and M. P. Zaletel, Majorana lattices from the quantized Hall limit of a proximitized spin-orbit coupled electron gas, Phys. Rev. B **99**, 115427 (2019).

[70] G. Chaudhary and A. H. MacDonald, Vortex-lattice structure and topological superconductivity in the quantum Hall regime, Phys. Rev. B **101**, 024516 (2020).

[71] K. Kudo, R. Nakai, and K. Nomura, Disorder-induced topological superconductivity in a spherical quantum-Hall–superconductor hybrid, Phys. Rev. B **110**, 035147 (2024).

[72] M. Tinkham, *Introduction to Superconductivity*, 2nd ed. (Dover Publications, New York, 2004).

[73] J. K. Jain, *Composite Fermions* (Cambridge University Press, New York, US, 2007).

[74] J. M. Murray and O. Vafek, Majorana bands, Berry curvature, and thermal Hall conductivity in the vortex state of a chiral *p*-wave superconductor, Phys. Rev. B **92**, 134520 (2015).

[75] T. Liu and M. Franz, Electronic structure of topological superconductors in the presence of a vortex lattice, Phys. Rev. B **92**, 134519 (2015).

[76] O. Vafek, A. Melikyan, M. Franz, and Z. Tešanović, Quasiparticles and vortices in unconventional superconductors, Phys. Rev. B **63**, 134509 (2001).

[77] F. Wu, T. Lovorn, E. Tutuc, I. Martin, and A. H. MacDonald, Topological insulators in twisted transition metal dichalcogenide homobilayers, Phys. Rev. Lett. **122**, 086402 (2019).

[78] J. Cai, E. Anderson, C. Wang, X. Zhang, X. Liu, W. Holtzmann, Y. Zhang, F. Fan, T. Taniguchi, K. Watanabe *et al.*, Signatures of fractional quantum anomalous Hall states in twisted $MoTe_2$, Nature (London) **622**, 63 (2023).

[79] H. Park, J. Cai, E. Anderson, Y. Zhang, J. Zhu, X. Liu, C. Wang, W. Holtzmann, C. Hu, Z. Liu *et al.*, Observation of fractionally quantized anomalous Hall effect, Nature (London) **622**, 74 (2023).

[80] Y. Zeng, Z. Xia, K. Kang, J. Zhu, P. Knüppel, C. Vaswani, K. Watanabe, T. Taniguchi, K. F. Mak, and J. Shan, Thermodynamic evidence of fractional Chern insulator in moiré $MoTe_2$, Nature (London) **622**, 69 (2023).

[81] F. Xu, Z. Sun, T. Jia, C. Liu, C. Xu, C. Li, Y. Gu, K. Watanabe, T. Taniguchi, B. Tong, J. Jia, Z. Shi, S. Jiang, Y. Zhang, X. Liu, and T. Li, Observation of integer and fractional quantum anomalous Hall effects in twisted bilayer $MoTe_2$, Phys. Rev. X **13**, 031037 (2023).

[82] K. Kang, B. Shen, Y. Qiu, Y. Zeng, Z. Xia, K. Watanabe, T. Taniguchi, J. Shan, and K. F. Mak, Evidence of the fractional quantum spin Hall effect in moiré $MoTe_2$, Nature (London) **628**, 522 (2024).

[83] Z. Lu, T. Han, Y. Yao, A. P. Reddy, J. Yang, J. Seo, K. Watanabe, T. Taniguchi, L. Fu, and L. Ju, Fractional quantum anomalous Hall effect in multilayer graphene, Nature (London) **626**, 759 (2024).

[84] Z. Dong, A. S. Patri, and T. Senthil, Theory of quantum anomalous Hall phases in pentalayer rhombohedral graphene moiré structures, Phys. Rev. Lett. **133**, 206502 (2024).

[85] J. Dong, T. Wang, T. Wang, T. Soejima, M. P. Zaletel, A. Vishwanath, and D. E. Parker, Anomalous Hall crystals in rhombohedral multilayer graphene. I. Interaction-driven Chern bands and fractional quantum Hall states at zero magnetic field, Phys. Rev. Lett. **133**, 206503 (2024).

[86] B. Zhou, H. Yang, and Y.-H. Zhang, Fractional quantum anomalous Hall effect in rhombohedral multilayer graphene in the moiréless limit, Phys. Rev. Lett. **133**, 206504 (2024).

[87] Y. H. Kwan, J. Yu, J. Herzog-Arbeitman, D. K. Efetov, N. Regnault, and B. A. Bernevig, Moiré fractional Chern insulators III: Hartree-Fock phase diagram, magic angle regime for Chern insulator states, the role of the moiré potential, and Goldstone gaps in rhombohedral graphene superlattices, Phys. Rev. B **112**, 075109 (2025).